IET Microwaves, Antennas & Propagation

Research Article

IET Journals
The Institution of Engineering and Technology

Enhancing the performance of defected ground structure type near-field radiofrequency WPT system by coupled-line impedance matching

ISSN 1751-8725
Received on 2nd March 2020
Revised 14th June 2020
Accepted on 23rd June 2020
E-First on 29th July 2020
doi: 10.1049/iet-map.2020.0217
www.ietdl.org

Shalin Verma[1] ✉, *Dinesh Rano*[1], *Mohammad Hashmi*[1,2]

[1]*Department of Electrical and Communication Engineering, IIIT Delhi, New Delhi 110020, India*
[2]*School of Engineering and Digital Sciences, Nazarbayev University, Nur-Sultan, 01000, Kazakhstan*
✉ *E-mail: shalinv@iiitd.ac.in*

Abstract: This study reports, for the first time, the use of coupled-line-based impedance matching in wireless power transfer (WPT) system. The transmitter and receiver of the WPT system are realised by microstrip feed line and symmetric coupled line at the top plane. The ground plane is realised with triangular-shaped defect along with the excitation slot mounted by an external capacitor. The defect in the ground plane and the external capacitor regulate the resonant frequency and also enable miniaturisation of the WPT system. The design is augmented with a systematic analytical approach for impedance matching and a simplified design procedure for the WPT system. A novel equivalent circuit model consisting of parallel LC network and coupled lines is also developed for the evaluation of the proposed WPT system design technique. A prototype of the system operating at 300 MHz developed on Rogers RO4350B substrate achieves a peak efficiency of 80% at a transmission distance of 17 mm. An excellent agreement between the measured and the electromagnetic simulated results is a testament of the robustness of the proposed design technique. Furthermore, evaluation of the commonly used WPT-related figure of merit shows significant enhancement when compared to the existing state of the art.

1 Introduction

A wide range of applications and their reliance on wireless power transfer (WPT) have been discussed by seminar reports and papers [1, 2]. This has led to a renewed interest in the WPT technology and systems as it has the potential to bring a paradigm shift in the design and development of devices for applications such as internet of things, wireless sensor networks, wireless body area network, electric vehicles etc. [3–5]. Moreover, a literature survey reveals that a number of WPT-related research papers in the 300–700 MHz band have been reported in the last few years. This covers many applications such as wearable devices, implant sensors, portable electronic gadgets and drug delivery systems [6–11].

It is imperative to note that the existing radiofrequency WPT systems can be distinctly categorised based on different transmission ranges such as short-range WPT-employing inductive (magnetic fields) coupling [12], mid-range WPT-employing resonant inductive coupling, external capacitors [13] and far-field WPT-using antenna at microwave frequency [14]. In terms of WPT system efficiency, a key metric, the inductive coupling-based techniques exhibit the highest efficiency followed by the capacitive coupling, the resonant inductive coupling and the far-field technique [13, 15]. It can be attributed to the fact that the capacitive coupling leads to small capacitance in the capacitive gap while the resonant coupling suffers from larger separation distance and hence lower efficiency [16, 17]. Similarly, the efficiency of the far-field power transfer is severely impacted by the loss in power due to relatively large transmission distance and loss in the rectification stage [14]. Overall, the resonant inductive techniques exhibit a very good trade-off between the system efficiency and power transmission range and therefore, find traction for many low-power applications [17].

The defected ground structure (DGS)-based resonant inductive technique is getting popular due to its versatility in the design of WPT systems [18–20]. Apparently, impedance matching plays a central role in achieving good WPT system efficiency. There are numerous techniques that have been proposed and most of these rely on shorting of external capacitor between the transmission line stub at the top plane and DGS resonator in the ground plane for enhancing WPT system efficiency [17, 21–23]. However, this approach leads to increased system complexity and reduced robustness. Furthermore, approach such as a double-stub matching technique can potentially address the above concerns but at the expense of large system size and reduced system efficiency [24]. Therefore, this approach essentially defeats the purpose of miniaturised WPT system with optimum efficiency and improved performance metrics.

This paper, therefore, presents a new coupled-line-based impedance matching technique, whereby symmetric coupled lines on the top plane of the DGS resonator are utilised, for the enhancement of WPT system efficiency. The utilisation of coupled line in impedance matching provides wideband matching performance which can be convenient in the case of any mismatch during the development of equivalent circuit of the WPT system and then in the practical realisation [25]. This is one of the key benefits of coupled-line matching over other matching techniques such as the open stub technique, exhibiting narrow band performance, used in the design of WPT systems [17, 21]. Furthermore, the coupled-line matching technique ensures perfect matching for wide range of input impedance (Z_{in}) to source impedance (Z_S) owing to the presence of even- and odd-mode characteristic impedances and the possibility to readily engineer them according to the need. This results in an improved and more versatile impedance matching and the eventual enhancement in the efficiency and other performance metrics. Furthermore, the choice of the triangular-shaped defect in the ground plane of the DGS resonator is regulated by the possibility of higher inductance which aids in reaching the resonance readily while keeping the goal of miniaturisation as a perspective.

The next section revisits the modelling and design of triangular-shaped DGS and realisation of its filter characteristics. Section 3 presents the realisation of the WPT system incorporating coupled lines and the adopted design strategy using the equivalent circuit model. Subsequently, experimental evaluation of the proposed technique and comparisons with the existing state-of-the-art is included in Section 4, while Section 5 concludes the paper.

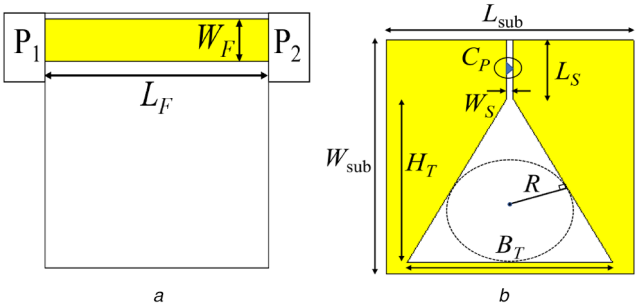

Fig. 1 *Structure of DGS resonator*
(a) Top plane, ***(b)*** Bottom plane

Table 1 Design parameters of triangular DGS resonator

Design parameters	Dimensions	Design parameters	Dimensions
L_F, mm	20	B_T, mm	16.6
W_F, mm	3.28	L_S, mm	5
L_{sub}, mm	20	W_S, mm	0.5
W_{sub}, mm	20	L_P, nH	24.64
H_T, mm	14	C_P, pF	11.3

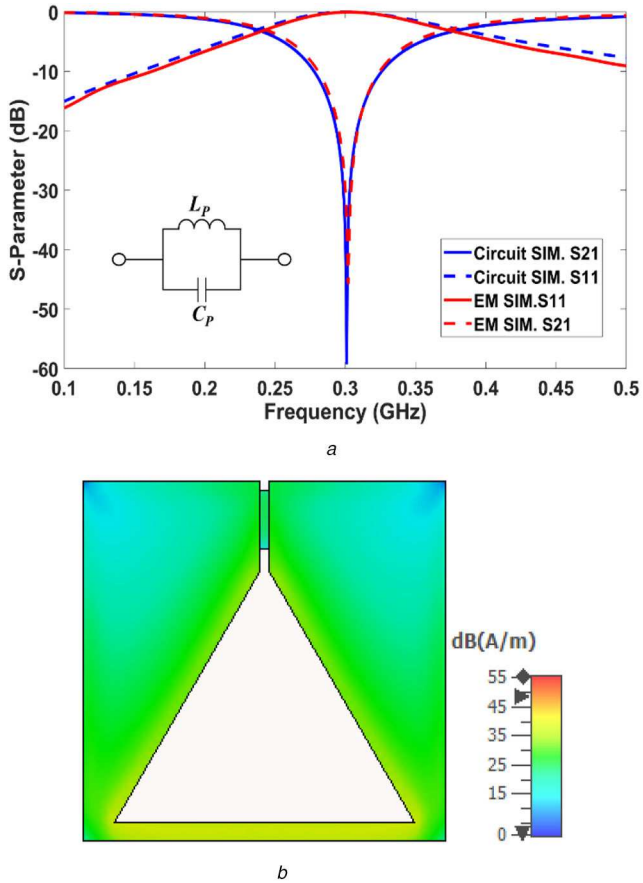

Fig. 2 *Band-stop performance of triangular DGS resonator*
(a) S-parameter plot of EM and circuit simulations, ***(b)*** EM simulated surface current distribution on the DGS surface

2 Triangular-shaped DGS resonator

2.1 Design and analysis

The triangular-shaped DGS resonator, depicted in Fig. 1, operating at a frequency of 300 MHz is realised on Rogers RO4350B having $\varepsilon_r = 3.66$, substrate thickness $h_{sub} = 1.524$ mm and metal thickness $t = 35$ µm. The top layer of the substrate is a 50 Ω microstrip feed line, of length L_F and width W_F, and is connected to lumped ports P1 and P2 as shown in Fig. 1*a*. The ground plane of overall length L_{sub} and width W_{sub}, shown in Fig. 1*b*, consists of a triangular defect of height H_T and base B_T with an internal angle of 60°, and excitation slot of length L_S and width W_S. The excitation slot of the resonator is mounted with an appropriate external capacitor C_P to achieve the desired operating frequency. Furthermore, the electromagnetic (EM) simulation is carried out in the computer simulation technology (CST) microwave studio based on two different scenarios. First, without C_P, the DGS resonator achieves resonance characteristics at 1.6 GHz. In the second case, the C_P is incorporated so as to fulfil the requirements of physical size (20×20 mm^2) restriction and target frequency. Subsequently, optimisations are carried out by increasing the height of the triangular defect in the ground plane so that the electrical length increases and this in turn reduces the resonant frequency. The optimised design parameters of the chosen triangular DGS resonator are listed in Table 1.

The developed resonator is then modelled as an equivalent parallel resonant LC circuit, shown in Fig. 2*a*, to aid in the expedited design and optimisation. The inductance L_P, contributed by the current flowing along the periphery of triangular-shaped DGS, and the capacitance C_P, representing the capacitor mounted on the excitation slot, are computed using (1) and (2) [22, 26]. These are key elements in creating the band-stop (ω_o) characteristics for the resonator

$$L_P = \frac{\mu_o P}{2\pi}\left[\ln\left(\frac{2P}{R}\right) + 0.25 - \ln\left(\frac{P^2}{A}\right)\right] \quad (1)$$

$$C_P = \frac{1}{\omega_o^2 L_P} \quad (2)$$

$$R_{DGS} = \mathrm{Re}(Z_{11}) \quad (3)$$

$$Q_U = \frac{\omega_o L_P}{R_{DGS}} \quad (4)$$

In the above expression, μ_o is the magnetic permeability of free space ($4\pi \times 10^{-7}$ H/m), P is the perimeter of the triangular DGS, R is the inscribed circle radius and A is the area of the DGS triangle. In general, L_P and C_P are in the range of nanohenry (nH) and picofarad (pF). The resistance R_{DGS}, expressed in (3), represents the losses in the DGS resonator [27]. This is obtained from one port Z-parameter (Z_{11}) EM simulation by removing the microstrip feed line from the top plane and then substituting a lumped port in the excitation slot. Finally, the unloaded quality factor (Q_U) of the resonator, expressed in (4), relies on the R_{DGS} and enables the determination of the losses in the resonator and the identification of efficiency of WPT system [21]. The values of inductance and capacitance extracted from (1) and (2) are substituted in the LC equivalent circuit and simulation is carried out in advanced design system (ADS) for comparing the results obtained in ADS and CST environments at the operating frequency of 300 MHz.

The S-parameter plot obtained from both circuit simulation and the EM simulation, Fig. 2*a*, compare favourably and thus the reliability of the developed circuit model is validated. In addition, the EM simulation is used to obtain the surface current distribution, of EM wave on the surface of the triangular-shaped DGS as shown in Fig. 2*b*. It can be seen that the surface current flowing around the periphery of the triangular defect perturbs the field propagating through the microstrip feed line at the operating frequency.

2.2 Investigation of DGS geometries

The layout of four different DGS shapes, namely triangular geometry, rectangular geometry, square geometry and circular geometry) are shown in Figs. 3*a–d*, respectively. Here, the comparison between four different DGS geometries is performed on the basis of similar design parameters. The design parameters of the proposed triangular DGS resonator such as substrate material,

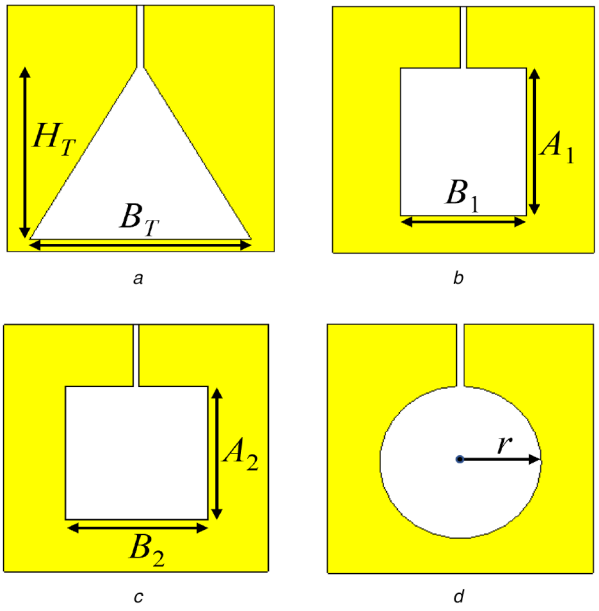

Fig. 3 *Layout of four different DGS geometries*
(a) Triangular geometry, ***(b)*** Rectangular geometry, ***(c)*** Square geometry, ***(d)*** Circular geometry

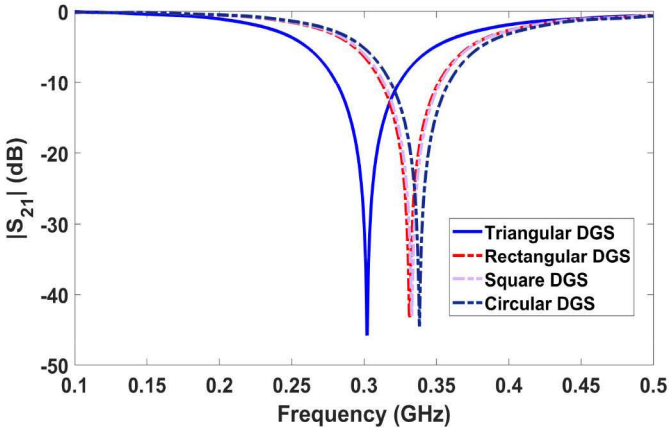

Fig. 4 *Comparison of EM simulated $|S_{21}|$ plot of triangular, rectangular, square and circular-shaped DGS resonator*

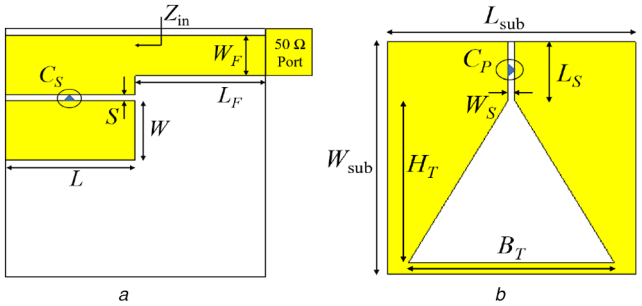

Fig. 5 *Use of coupled lines in the modified DGS resonator structure in the proposed WPT system*
(a) Top plane, ***(b)*** Bottom plane

overall length L_{sub} and width W_{sub}, microstrip feed line of length L_F and width W_F, excitation slot of length L_S and width W_S, and external capacitor C_P are utilised to design the other three DGS resonators. In addition, the area of rectangular defect ($A_1 \times B_1 = 12 \times 9.7$ mm^2), square defect ($A_2 \times B_2 = 10.8 \times 10.8$ mm^2) and circular defect ($\pi x r^2 = \pi x(6.1)^2$ mm^2) is almost similar to the area occupied by the triangular defect ($0.5 \times H_T \times B_T = 116.2$ mm^2).

The EM simulated $|S_{21}|$ plot, as shown in Fig. 4, demonstrates that the triangular defect has the highest inductance value in comparison to rectangular-, square- and circular-shaped defects in a similar area as can be deduced from the smallest resonant frequency for the triangular DGS. This high inductance value of the triangular defect is due to the tapered side width and length which increases the physical length of the defect to a greater degree. The increased physical length of the defect results in the increased electrical length and therefore aids in achieving resonance more readily.

3 Proposed WPT system

3.1 WPT system design

The proposed DGS-based WPT system makes use of the modified resonator shown in Fig. 5*a*. It consists of a microstrip feed line followed by a symmetric defected coupled line of length L, width W and gap S on the top plane. The length of the microstrip feed line

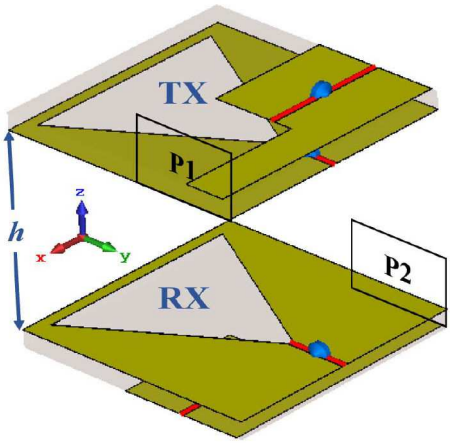

Fig. 6 *Back-to-back view of the proposed DGS-based WPT system including the direction of flow*

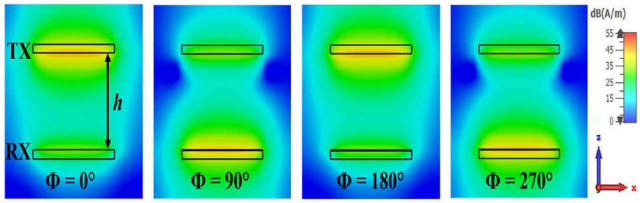

Fig. 7 *EM simulated magnetic field distribution of the proposed DGS-based WPT system at 300 MHz at plane Y = 0*
(a) Φ = 0°, ***(b)*** Φ = 90°, ***(c)*** Φ = 180°, ***(d)*** Φ = 270°

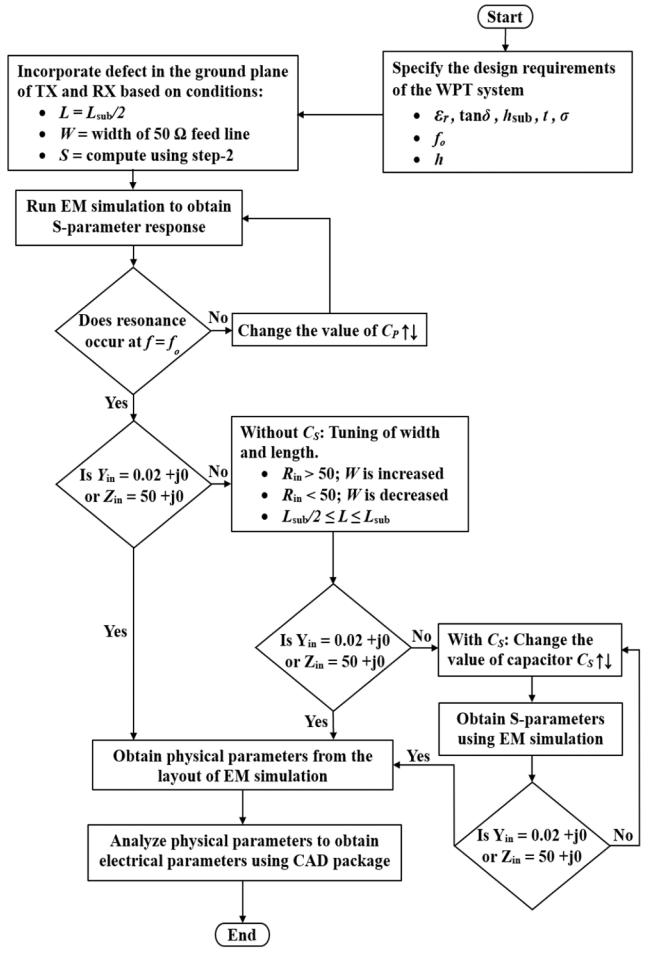

Fig. 8 *WPT system design flow using the coupled line with DGS*

on the top plane in this design is reduced to half the total length of the substrate. This makes sure that the excitation slot of DGS resonator lies exactly below the centre of the substrate which acts as a location for analysing the input impedance (Z_{in}). The impedance matching network is also substituted at that point in the eventual WPT system. Moreover, an external capacitor C_S mounted between the energised coupled-line segment and the passive coupled-line segment provides an additional capacitance for impedance matching. The C_S is required when the capacitance realised by the coupled line is not sufficient for a perfect match at the desired resonant frequency. Both the C_S and the coupled line of length L provide the frequency tuning capability and thus help in finely adjusting the resonance frequency close to the operating frequency. Furthermore, the ground plane, shown in Fig. 5*b*, is exactly similar to the ground plane of the original resonator described in Section 2 and hence the design parameters for the bottom plane remain the same except the capacitor C_P as explained in Section 3.2.

The proposed WPT system is realised by placing two modified resonators back to back separated by a distance h as shown in Fig. 6. Apparently, the resonators are symmetric and have coupled line on the top plane. One end of the microstrip feed line is connected to ports P1 and P2 while the other end of both the resonators is left open. The separation distance h between the two resonators transforms the band-stop characteristics of the DGS resonators into band-pass characteristics. It facilitates power transfer from TX to RX at the operating frequency (300 MHz in this instance). The power transfer between the two DGS resonators follows the principle of non-radiative near-field resonant inductive coupling. This can also be inferred from Fig. 7 which shows the EM simulated magnetic field current distribution plot of the proposed DGS-based WPT system at different phases Φ (0°, 90°, 180° and 270°).

3.2 Systematic design procedure

The proposed WPT system includes the effect of DGS in the coupled lines and therefore the associated design process of this modified resonator and hence the full WPT system is different as depicted in Fig. 8. The design flow considers both the scenarios whether C_S is required or not for achieving the perfect impedance matching. The process is explained in simplified steps below by considering TX. Similar steps are required for resonator employed in the design of RX.

Step 1: Specify the design requirements of the WPT system i.e. the operating frequency f_o, size ($L_{sub} \times W_{sub}$) and choose the substrate parameters such as relative permittivity (ε_r), loss tangent (tanδ), height (h_{sub}), thickness (t) and conductivity (σ).

Step 2: Using computer aided design (CAD) tool such as ADS, determine the physical parameters of coupled line namely the width (W), the gap (S) to fulfil the coupling factor (C) and the length (L). For practical WPT systems, C is in the range of -10 dB $> C > -20$ dB and depends on fabrication complexity and impedance matching issues. For the determination of L, assume $L = L_{sub}/2$.

Step 3: Consider the initial value of transmission distance $h = L_{sub}/2$. Then the transmission distance is varied until maximum power transfer efficiency at the critical coupling.

Step 4: Utilise the physical parameters of coupled line computed in step 2 along with the defect in the ground plane of the TX and RX.

Step 5: Tune L and W of the coupled line until the desired value of Z_{in} ($= 50 + j0$) is obtained. For length, maintain $L_{sub}/2 \leq L \leq L_{sub}$ while tuning to achieve the imaginary part of Z_{in} equal to zero. For $R_{in} > 50\ \Omega$, increase the W of coupled line whereas for $R_{in} < 50\ \Omega$, decrease the W of the coupled line to obtain $\mathrm{Re}(Z_{in}) = 50\ \Omega$. Furthermore, if the desired value of Z_{in} is not obtained by tuning L and W then external capacitor C_S is required to achieve perfect matching.

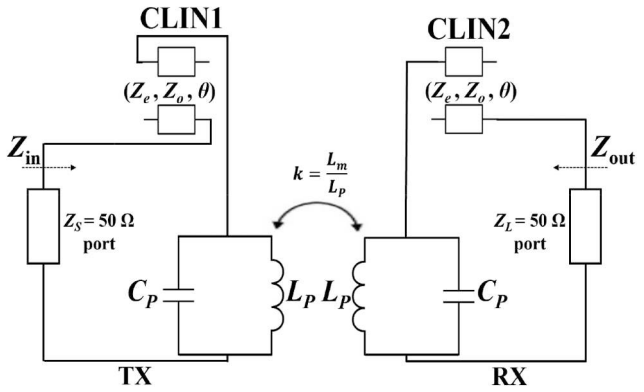

Fig. 9 *Equivalent circuit of DGS WPT system with coupled line-based impedance matching*

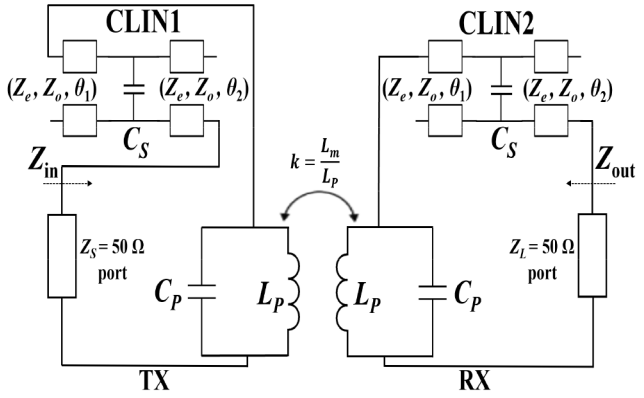

Fig. 10 *Equivalent circuit of DGS WPT system using coupled lines impedance matching and an external capacitor (C_S)*

Step 6: Once Z_{in} is matched to the port impedance of 50 Ω, use the optimised physical parameters obtained from the EM simulation to extract electrical parameters. Finally, utilise these electrical parameters to generate the equivalent circuit for system evaluation and performance validation.

An important aspect to consider during the design of the WPT system is that a shift in the resonance frequency from the design frequency is very common. It is due to the effect of mutual coupling between the transmitter and receiver caused by the separation distance. This issue can be overcome by tuning the C_P until the design frequency (f_o) is obtained.

3.3 Equivalent circuit modelling

The proposed WPT system can be modelled by its equivalent circuits shown in Figs. 9 and 10. Apparently, there are slight differences in these two and the subsequent descriptions provide clarity in this regard. The circuit in Fig. 9 consists of two symmetric DGS resonators modelled by equivalent parallel LC circuit and coupled lines. Both the resonators are coupled through mutual inductance L_m and hence the coupling coefficient k [21].

In these equivalent circuits, the coupled lines (CLIN1 and CLIN2) between the port terminations and the TX–LC circuit and RX–LC circuit takes care of the impedance mismatches between the Z_{in} and the Z_S. The equivalent circuit model in Fig. 10 depicts the scenario when the external capacitor C_S is required for matching. Once again, the arrangement of two similar coupled lines is used between the port termination and both TX-LC and RX-LC circuits. The two coupled lines are connected in parallel by capacitor C_S so that the electrical length (θ_1 and θ_2) of both the lines combine to give the total electrical length (θ). For design ease, the electrical length of both the coupled lines is distributed in equal proportion.

The coupling coefficient (k) between the TX and RX resonator is plotted with respect to the transmission distance in Fig. 11. The

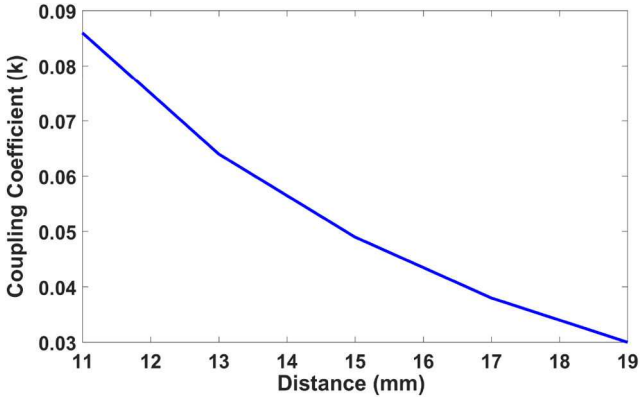

Fig. 11 *Variation of coupling coefficient w.r.t. distance*

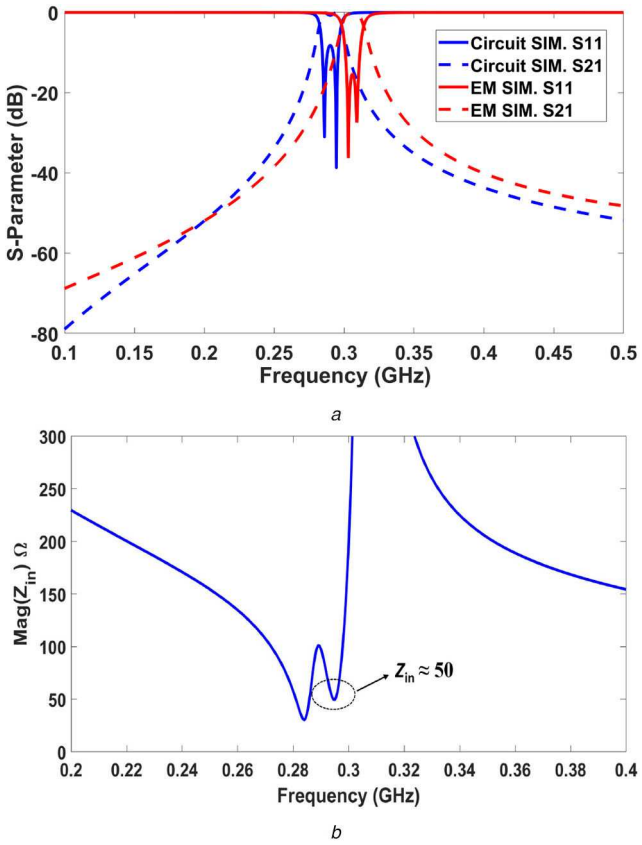

Fig. 12 *EM simulation and circuit simulation plot of the proposed WPT system*

(a) Comparison of EM simulation and circuit simulation S-parameters, ***(b)*** Magnitude of input impedance versus frequency

value of the coupling coefficient is recorded for increasing the value of transmission distance from 11 to 19 mm at the operating frequency. It can be seen from the plot that the coupling is maximum at 11 mm and minimum at 19 mm and it is in line with the established theory. Moreover, keeping the overall size of the WPT system in perspective, the range of separation distance is kept between 11 and 19 mm due to the fact that the WPT system is in the over-coupled region within this range. The coupling becomes very large <11 mm, whereas it reduces and eventually reaches close to zero at a separation distance >19 mm. Both these scenarios lead to degradation of the WPT system efficiency. In this analysis, the points in the range nearer to the critically coupled distance have been considered.

Subsequently, the circuit model is simulated in ADS. It can be seen in Fig. 12*a* that the circuit simulation results, although exhibit similar shape, experience some variation from the EM simulation results. It occurs due to the slight overlap of triangular defect and excitation slot in the ground plane with the coupled line on the top

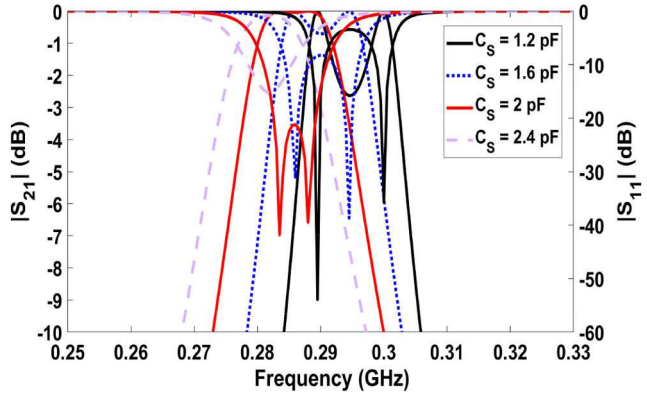

Fig. 13 *Circuit simulated S-parameter for various C_S values*

Table 2 Optimised design parameters of WPT system using triangular-shaped DGS and coupled lines

Design parameters	f_o = 300 MHz	f_o = 700 MHz	Design parameters	f_o = 300 MHz	f_o = 700 MHz	Design parameters	f_o = 300 MHz	f_o = 700 MHz
L_{sub}, mm	20	20	$\rho = Z_e/Z_o$	1.5	1.59	C_P, pF	9.1	2
W_{sub}, mm	20	20	θ, deg	6.09	11	C_S, pF	1.6	—
L_F, mm	10	10	R_{in}, Ω	49.7	49.5	R_{DGS}, Ω	0.088	0.159
W_F, mm	3.28	3.28	X_{in}, Ω	0.4	0.9	Q_U	530	549.5
L, mm	10	8	L_S, mm	5	5	L_m, nH	0.971	0.92
W, mm	4.8	2	W_S, mm	0.5	0.5	k	0.0379	0.046
S, mm	0.5	0.8	H_T, mm	14	11	h, mm	17	17
Z_e, Ω	45	79.3	B_T, mm	16.6	14.2	η, %	83	94
Z_o, Ω	30	49.88	L_P, mm	24.64	19.8	—	—	—

plane. The effect of triangular defect and excitation slot on the coupled line has not been considered in the circuit simulation.

In essence, this overlap leads to a reduction in the physical length and the electrical length of the coupled line. Furthermore, the overlap increases the even-mode impedance (Z_e) substantially and the odd-mode impedance (Z_o) marginally. Apparently, the reduction in the physical length results in the decrease of gap capacitance. As a consequence, the reduced gap capacitance along with the increased even- and odd-mode impedances leads to an increase in the resonance frequency and therefore we observe the shift between the circuit simulation and EM simulation results. Moreover, the shift in the circuit simulation result can also be attributed to the anomaly in substrate parameters, such as losses, not taken into consideration while developing the equivalent circuit model. In addition, small frequency split can also be observed in both the EM simulation and circuit simulation results and these convey the transformation from the over coupled to critically coupled region.

Furthermore, a swept frequency response for input impedance (Z_{in}) using the circuit model gives the outcome presented in Fig. 12*b*. It can be inferred that the desired impedance of 50 Ω is obtained at 295 MHz and once again it demonstrates the effectiveness of the model in cross-validation of the performance.

In addition, the proposed equivalent circuit is very effective in achieving the desired resonant frequency quickly. The impedance matching obtained using the coupled line and the external capacitor C_S is depicted in Fig. 13. The value of external capacitor C_S is varied between 1.2 and 2.4 pF to study the wideband matching performance of the proposed WPT system. It is apparent that the increase in C_S leads to a shift in the resonance frequency downwards while still maintaining decent power transfer. Just for clarity, an optimum wideband matching performance ($|S_{11}| < -30$ dB), not given here, is maintained between 283 and 300 MHz for three different C_S, i.e. 2,1.6 and 1.2 pF but degrades at larger C_S of 2.4 pF.

To understand the effectiveness of the proposed design and modelling approach, the WPT system is also designed at frequency 700 MHz. The performance and parameters were easily optimised using the proposed approach and Table 2 lists them for ready reference.

4 Measurement results and discussion

4.1 Performance evaluation

The prototype in Fig. 14*a* depicts the bottom and top planes of the proposed resonator. The realisation of WPT system requires back-to-back connection of two such resonators. One of the resonators acts as a TX and the other as RX. The resonators are separated by plastic foam, as shown in the measurement setup of Fig. 14*b*, to maintain a distance h of 17 mm between them for optimal efficiency. This optimal distance was achieved in simulation. The measured S-parameter results obtained for the WPT system are plotted in Fig. 15. The result clearly shows resonance characteristics at $f_o = 300.5$ MHz with $|S_{21}| = -1$ dB and $|S_{11}| = -21$ dB. The measured result, although excellent, shows slight variation in the resonance frequency from the operating frequency of 300 MHz. This occurs due to the tolerances of the capacitors C_P and C_S (part numbers CBR04C919B5GAC and CBR04C169B5GAC) and the parasitic effects inherent in the designed system. In addition, other factors such as the inset of plastic foam which adds on to the permittivity, and the in-house fabrication which introduces losses such as soldering loss, connector loss etc. also introduce some anomaly.

To overcome the shift in the frequency, capacitor values with low tolerances and frequency tuning should be used. Moreover, it can be seen that the obtained bandwidth from measurement is larger when compared to the EM simulation. This once again can be attributed to the losses in the connector, substrate, and metal which decrease the quality factor of the WPT system.

The measured efficiency (η_{WPT}) of the developed WPT system, computed using (5) [24], is 80% at 300.5 MHz. Subsequently, the measured efficiency of the WPT system at the operating frequency is validated using Anritsu MS2720 T spectrum master. Here, an input power of 0 dBm at 300.5 MHz is fed to the transmitter DGS resonator and the spectrum of the output power is recorded at the receiver DGS resonator as shown in Fig. 16. The received output

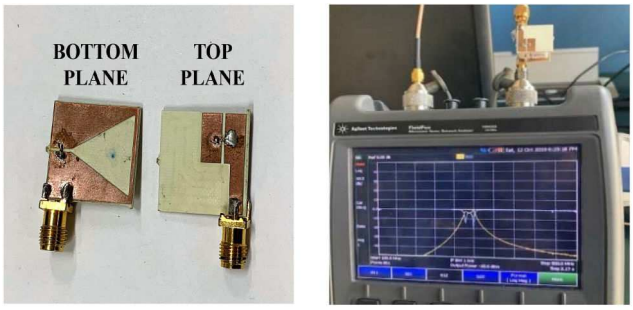

a *b*

Fig. 14 *Prototype and measurement*
(a) Bottom and top sides, ***(b)*** Measurement setup

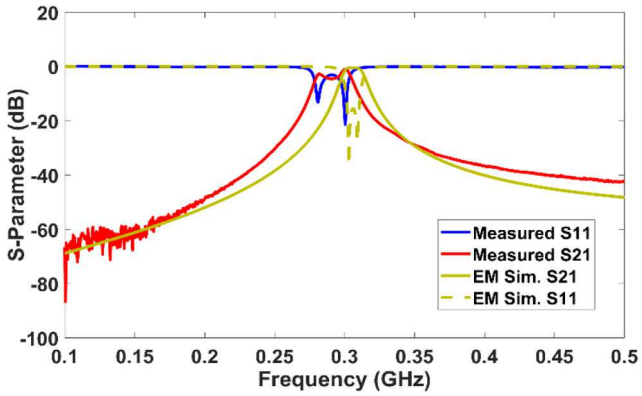

Fig. 15 *Measured and EM simulated S-parameters*

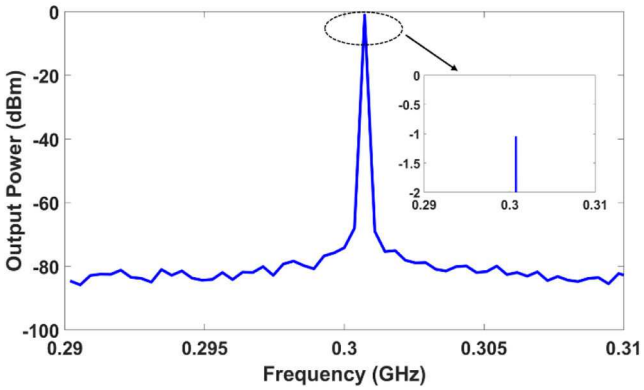

Fig. 16 *Received output power measured using power spectrum analyser at the design frequency*

Table 3 Performance comparison of proposed WPT system with the state-of-the-art designs

WPT system	Matching technique	f_o, GHz	Size, mm	h, mm	η_{WPT}, %	FoM
[17]	open stub	0.27	20 × 20	11	71	0.390
[21]	open stub	0.3	20 × 20	13	68	0.442
[28]	open stub	0.88	23 × 12	8	70	0.34
[29]	open stub	1.43	20 × 20	3.5	85	0.148
this work	coupled line	0.3	20 × 20	17	80	0.68

power at 300.5 MHz is −1 dBm over 17 mm separation distance, respectively. The ratio of output power and input power gives similar efficiency as computed by (5) and thus provides confidence in the measured efficiency value obtained using vector network analyser (VNA) setup. This obtained efficiency is excellent and far superior to other recently reported DGS-based WPT systems listed in Table 3. This inference is made by comparing and trading-off various parameters such as resonant frequency, size, power transmission distance and efficiency

$$\eta_{WPT} = \frac{|S_{21}|^2}{1-|S_{11}|^2} = \frac{\text{Transferred Power (TP)}}{1-|S_{11}|^2} \quad (5)$$

$$\text{FoM} = \frac{\eta_{WPT} \times h}{\sqrt{\text{Size}}} \quad (6)$$

The proposed WPT system is also compared on the basis of figure of merit (FoM) calculated using (6) [24]. The FoM provides a platform for estimating the performance of various WPT systems by considering the effects of distance, efficiency and the size of the WPT system. It can be seen in Table 3 that the proposed design exhibits an FoM of 0.68 which is significantly improved when compared to other reported systems operating in the same frequency range.

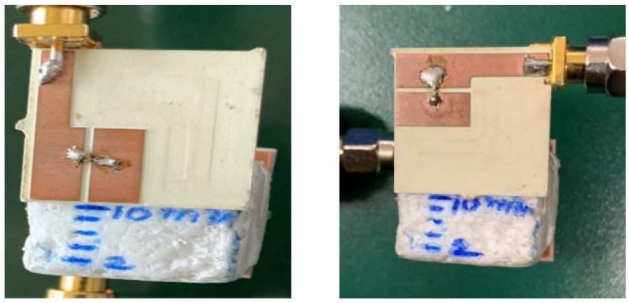

a b

Fig. 17 *Lateral misalignment of prototype*
(a) Lateral shift in the *X*-direction, ***(b)*** Lateral shift in the *Y*-direction

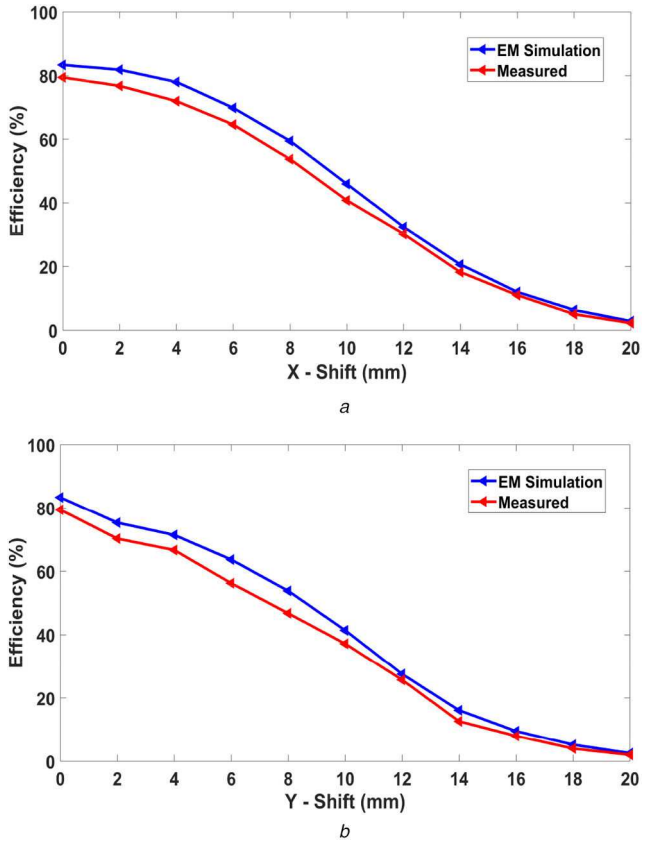

Fig. 18 *Effect of lateral misalignment*
(a) Shift in the *X*-direction, ***(b)*** Shift in the *Y*-direction

4.2 Misalignment study

The WPT system can be greatly impacted by lateral and angular misalignments between the TX and RX. In order to understand this impact, the TX and RX are laterally shifted along the horizontal (*X*-axis) direction and then along the vertical (*Y*-axis) direction as depicted in Figs. 17*a* and *b*, respectively. The effect of lateral shift on efficiency is studied and the obtained results are shown in Figs. 18*a* and *b*.

For Fig. 18*a*, the result is recorded when the RX is shifted along the *X*-axis between 0 and 20 mm with a step-size of 2 mm. At 0 mm, the RX is in the line of sight and is perfectly aligned with the TX, whereas 20 mm is the maximum misalignment. It is apparent in Fig. 18*a* that the efficiency is maximum at no misalignment (i.e. misalignment of 0 mm) and degrades with the increase in misalignment until it approaches zero at 20 mm in this case. The results of misalignment along the *Y*-axis, shown in Fig. 18*b*, convey that the maximum and minimum efficiencies follow the similar pattern.

It can be deduced from Figs. 18*a* and *b* that the degradation of efficiency with the shift in *X*- and *Y*-directions is almost similar and consistent. These results identify that the proposed design achieves an efficiency of >50% even with lateral misalignment of 6–8 mm

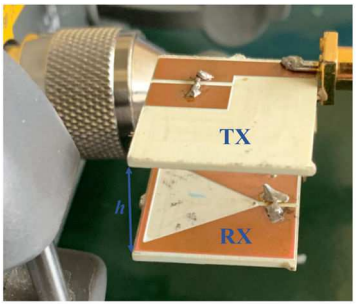

Fig. 19 *Three-dimensional representation of angular rotation of RX position at 90°*

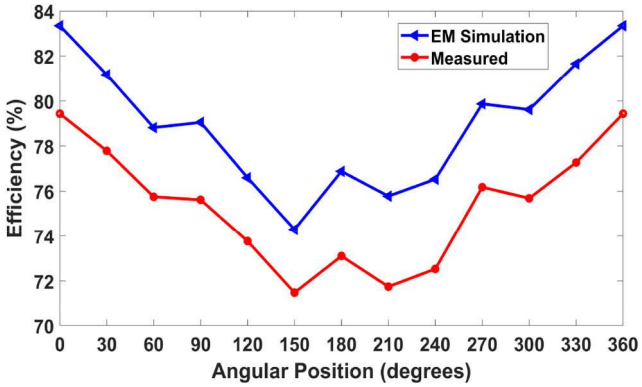

Fig. 20 *Effect of angular misalignment of RX on efficiency*

and this is far superior to an earlier reported H-shaped DGS-based WPT system with an identical lateral shift in the *X*-direction [21]. Furthermore, the proposed system exhibits similar efficiency when compared to the H-shaped DGS-based WPT system when misalignment occurs in the *Y*-direction. The consistency in the achieved results for the proposed WPT system can be attributed to the excellent matching achieved by incorporating the coupled-line-based impedance transformation technique.

Subsequently, the angular misalignment for various angular positions between 0° and 360° of TX and RX are studied. One such case of the angular orientation of the RX position at 90° is shown in Fig. 19. It can be seen in Fig. 20 that the EM simulated efficiency and the measured efficiency follows a similar pattern with some anomaly due to soldering loss, connector loss etc. during the prototyping process. It also coveys that the efficiency is not greatly impacted by the angular misalignment of TX and RX. It once again significantly improves the outcome reported for the H-shaped DGS WPT system [21].

In brief, it is safe to convey that the proposed system is immune to the variation in the angular position of the RX considering that there is no major drop in system efficiency. This is due to the fact that the maximum area of coupled lines of the RX is in the line of sight with the TX unlike the two cases of lateral shifts. Notably, it can be seen that the measured efficiency for the 90° orientation is close to 76% and this is excellent for any practical situation requiring TX and RX to be misaligned by 90°.

5 Conclusion

A new technique using symmetric coupled lines for impedance matching and miniaturisation of WPT systems has been proposed. First, the theoretical foundations are developed which are subsequently validated through EM simulation, circuit simulation and measurement results. The proposed technique is frequency scalable and exhibits reduced complexity in fabrication through the introduction of surface-mounted capacitor between the coupled lines on a top plane to obtain perfect matching. The incorporation of the defect in the ground plane solves two different purposes namely miniaturisation of the overall WPT system and the achievement of the desired resonant frequency. The reported DGS-based WPT system using coupled lines takes an area of 20 × 20

mm^2 and achieves power transfer at 17 mm with 80% system efficiency. The designed system possesses superior FoM as compared to recent works and thus significantly improves the existing state of the art.

6 References

[1] Cost Action IC1301 Team: 'Europe and the future for WPT: european contributions to wireless power transfer technology', *IEEE Microw. Mag.*, 2017, **18**, (4), pp. 56–87

[2] Agarwal, K., Jegadeesan, R., Guo, Y.*, et al.*: 'Wireless power transfer strategies for implantable bioelectronics', *IEEE Rev. Biomed. Eng.*, 2017, **10**, pp. 136–161

[3] Rano, D., Hashmi, M.: 'Extremely compact EBG-backed antenna for smartwatch applications in medical body area network', *IET Microw. Antennas Propag.*, 2019, **13**, (7), pp. 1031–1040

[4] Kung, M., Lin, K.: 'Dual-band coil module with repeaters for diverse wireless power transfer applications', *IEEE Trans. Microw. Theory Tech.*, 2018, **66**, (1), pp. 332–345

[5] Huh, J., Lee, S. W., Lee, W. Y.*, et al.*: 'Narrow-width inductive power transfer system for online electrical vehicles', *IEEE Trans. Power Electron.*, 2011, **26**, (12), pp. 3666–3679

[6] Xue, R. F., Cheng, K. W., Je, M.: 'High-efficiency wireless power transfer for biomedical implants by optimal resonant load transformation', *IEEE Trans. Circuits Syst. I*, 2013, **60**, (4), pp. 867–874

[7] Kang, S. H., Nguyen, V. T., Jung, C. W.: 'Analysis of MR-WPT using planar textile resonators for wearable applications', *IET Microw Anten. Propag.*, 2016, **10**, (14), pp. 1541–1546

[8] Lee, H. H., Kang, S. H., Jung, C. W.: '3D-spatial efficiency optimisation of MR-WPT using a reconfigurable resonator-array for laptop applications', *IET Microw. Antennas Propag.*, 2017, **11**, (11), pp. 1594–1602

[9] Hirai, J., Kim, T. W., Kawamura, A.: 'Study on intelligent battery charging using inductive transmission of power and information', *IEEE Trans. Power Electron.*, 2000, **15**, (2), pp. 335–345

[10] Ling, Z., Hu, F., Wang, L.*, et al.*: 'Point-to-point wireless information and power transfer in WBAN with energy harvesting', *IEEE Access*, 2017, **5**, pp. 8620–8628

[11] Soltesz, K., Sturk, C., Paskevicius, A.*, et al.*: 'Closed-loop prevention of hypotension in the heart beating brain-dead porcine model', *IEEE Trans. Biomed. Eng.*, 2017, **64**, (6), pp. 1310–1317

[12] Ye, Z. H., Sun, Y., Dai, X.*, et al.*: 'Energy efficiency analysis of U-coil wireless power transfer system', *IEEE Trans. Power Electron.*, 2016, **31**, (7), pp. 4809–4817

[13] Jang, B. J., Lee, S., Yoon, H.: 'HF-band Wireless power transfer system: concept, issues, and design', *Prog. Electromagn. Res.*, 2012, **124**, pp. 211–231

[14] Brown, W. C.: 'The history of power transmission by radio waves', *IEEE Trans. Microw. Theory Tech.*, 1984, **32**, (9), pp. 1230–1242

[15] Dai, J., Ludois, D. C.: 'Single active switch power electronics for kilowatt scale capacitive power transfer', *IEEE J. Emerg. Sel. Top. Power Electron.*, 2015, **3**, (1), pp. 315–323

[16] Ngo, T., Huang, A. D., Guo, Y. X.: 'Analysis and design of a reconfigurable rectifier circuit for wireless power transfer', *IEEE Trans. Ind. Electron.*, 2019, **66**, (9), pp. 7089–7098

[17] Verma, S., Rano, D., Hashmi, M.*, et al.*: 'A high Q dual E shaped defected ground structure for wireless power transfer applications'. IEEE Asia Pacific Microwave Conf., Kyoto, Japan, November 2019, pp. pp. 1435–1437

[18] Dautov, K., Hashmi, M., Nauryzbayev, G.*, et al.*: 'Recent advancements in defected ground structure based near-field wireless power transfer systems', *IEEE Access*, 2020, **8**, pp. 81298–81309

[19] Verma, S., Rano, D., Hashmi, M.: 'A novel dual band defected ground structure for short range wireless power transfer applications'. IEEE Wireless Power Transfer Conf., London, UK., 2019, pp. 188–191

[20] Sharaf, R., Abdel-Rahman, A. B., Abd El-Hameed, A. S.*, et al.*: 'A new compact dual-band wireless power transfer system using interlaced resonators', *IEEE Microw. Wirel. Compon. Lett.*, 2019, **29**, (7), pp. 498–500

[21] Hekal, S., Abdel-Rahman, A. B., Jia, H.*, et al.*: 'A novel technique for compact size wireless power transfer applications using defected ground structures', *IEEE Trans. Microw. Theory Tech.*, 2017, **65**, (2), pp. 591–599

[22] Saad, M. R., Tahar, F., Barakat, A.*, et al.*: 'Analysis of near field wireless power transfer using bow-tie defected ground structure'.2017 IEEE Asia Pacific Microwave Conf., Kuala Lumpur, Malaysia, 2017, pp. 495–498

[23] Barakat, A., Hekal, S., Pokharel, R.K.: 'Simple design approach for asymmetric resonant inductive coupled WPT systems using J-inverters'. IEEE Asia Pacific Microwave Conf., New Delhi, India, 2016, pp. 1–3

[24] Tahar, F., Barakat, A., Saad, R.*, et al.*: 'Dual band defected ground structures wireless power transfer system with independent external and inter-resonator coupling'. *IEEE Trans. Circuits Syst. II, Exp. Briefs*, 2017, **64**, pp. 1372–1376

[25] Jensen, T., Zhurbenko, V., Krozer, V.*, et al.*: 'Coupled transmission lines as impedance transformer', *IEEE Trans. Microw. Theory Tech.*, 2007, **55**, (12), pp. 2957–2965

[26] Grover, F. W.: '*Inductance calculations: working formulas and tables*' (Courier Corporation, New York, USA., 1946)

[27] Garg, R., Bahl, I., Bozzi, M.: '*Microstrip lines and slotlines*' (Artech House, Norwood, MA, USA., 2013)

[28] Malhotra, S., Hashmi, M.: 'Near-field WPT using defected ground structures for UHF RFID applications'. 2019 IEEE Int. Conf. on RFID Technology and Applications (RFID-TA), 2019, pp. 16–21

[29] Hekal, S., Abdel-Rahman, A. B., Jia, H.*, et al.*: 'Strong resonant coupling for short-range wireless power transfer applications using defected ground structures'. IEEE Wireless Power Transfer Conf., Boulder, CO, USA., 2015, pp. 1–4